POLITECNICO DI TORINO
Repository ISTITUZIONALE

414.7-Gbit/s Single-Aperture Dual-Polarization 287 GHz Wireless Link

Original
414.7-Gbit/s Single-Aperture Dual-Polarization 287 GHz Wireless Link / Dittmer, J., Pilori, D., Bhutani, A., Hilkert, A.-C., Mahmud, M.S., Gostner, F., Tessmann, A., Wagner, S., Nolte, L., Li, H., Koos, C., Zwick, T., Schmalen, L., Randel, S.. - In: IEEE TRANSACTIONS ON TERAHERTZ SCIENCE AND TECHNOLOGY. - ISSN 2156-342X. - ELETTRONICO. - (In corso di stampa), pp. 1-10. [10.1109/tthz.2026.3749414]

Availability:
This version is available at: 11583/3017427 since: 2026-11-03T06:22:28Z

Publisher:
IEEE

Published
DOI:10.1109/tthz.2026.3749414

Terms of use:

This article is made available under terms and conditions as specified in the corresponding bibliographic description in the repository

Publisher copyright

(Article begins on next page)

27 November 2026

This article has been accepted for publication in IEEE Transactions on Terahertz Science and Technology. This is the author's version which has not been fully edited and content may change prior to final publication. Citation information: DOI 10.1109/TTHZ.2026.3749414

414.7-Gbit/s Single-Aperture Dual-Polarization 287 GHz Wireless Link

J. Dittmer*, D. Pilori*, A. Bhutani, A.-C. Hilkert, Md S. Mahmud, F. Gostner, A. Tessmann, S. Wagner, L. Nolte, H. Li, C. Koos, T. Zwick, L. Schmalen, and S. Randel

***Abstract*—In this paper we experimentally investigate a coherent single-aperture dual-polarization wireless link operating at 287 GHz over a 56-m line-of-sight indoor path within the IEEE 802.15.3d frequency allocation. The transmitter employs photonic carrier generation by optical heterodyning in uni-traveling-carrier photodiodes, while reception is performed by two synchronized all-electronic intradyne front-ends implemented in 35 nm mHEMT technology. Using one dual-polarized antenna aperture at each end of the link, the system realizes polarization-division multiplexing without spatially separated wireless paths or multiple antenna pairs. A systematic comparison of dual-polarization QPSK, uniform 16-QAM, and probabilistically shaped 16-QAM with entropies of 3.5 and 3.8 bit/symbol is presented for symbol rates from 30 to 64 GBd. The results quantify the trade-off between robustness, spectral efficiency, and practical forward-error correction. QPSK maintains an average signal-to-noise-and-distortion ratio above 11 dB over the full symbol-rate range and supports 241.9 Gbit/s net throughput with low-overhead hard-decision FEC. At 64 GBd, uniform 16-QAM achieves the highest demonstrated net throughput of 414.7 Gbit/s after practical soft-decision LDPC decoding, whereas probabilistically shaped 16-QAM reaches 413.7 Gbit/s with reduced FEC overhead and increased decoding margin. These results demonstrate the feasibility of single-aperture, dual-polarization sub-terahertz wireless links at data rates exceeding 400 Gbit/s and provide insights into the modulation and coding trade-offs relevant to future high-capacity point-to-point systems.**

***Index Terms*—Terahertz communication, coherent optical communication, polarization-division multiplexing, probabilistic constellation shaping, quadrature amplitude modulation, quadrature phase-shift keying, wireless communication.**

I. Introduction

FUTURE sixth-generation (6G) communication networks are expected to support applications requiring wireless data rates well beyond those available in current communication systems [1]. Immersive extended-reality services, distributed artificial intelligence, autonomous transportation, cloud radio access networks, and wireless front- and backhaul infrastructures will require wireless links capable of transporting hundreds of gigabits per second while maintaining low latency and high reliability. While optical fiber remains the preferred solution whenever physical deployment is feasible, fiber installation is often costly, time-consuming, or impractical in rapidly deployable and reconfigurable network infrastructures. Consequently, sub-terahertz (sub-THz) wireless communication has emerged as one of the most promising technologies for realizing fiber-class wireless connectivity over short and medium distances [2], [3].

Among the available spectrum resources, the frequency range between 252.72 and 321.84 GHz standardized by IEEE 802.15.3d in 2017 provides nearly 70 GHz of contiguous bandwidth for point-to-point wireless communication [2]. Such unprecedented bandwidth enables symbol rates exceeding 60 GBd using conventional single-carrier modulation and allows transmission capacities far beyond those achievable in current millimeter-wave systems. However, practical communication in this frequency range remains challenging owing to severe free-space propagation loss, which scales with both transmission distance and carrier frequency, as well as atmospheric absorption, limited transmitter output power, finite receiver sensitivity, and the wide analog bandwidth required throughout the transceiver chain [4], [5]. As a consequence, highly directional high-gain antennas are generally required to establish wireless links over practical distances exceeding several meters. The resulting pencil-beam operation restricts current sub-THz systems primarily to fixed point-to-point deployments, including wireless backhaul, fronthaul, campus networks, and data-center interconnects.

The realization of high-capacity sub-THz transceivers has therefore become an active research topic. Electronic transmitter and receiver implementations based on SiGe BiCMOS, CMOS, InP, and GaAs technologies offer increasing levels of integration and have demonstrated continuous improvements in output power, bandwidth, and receiver sensitivity over the last years [5]. In parallel, optoelectronic transmitter architectures based on optical heterodyne generation have attracted considerable interest because they leverage mature photonic technologies originally developed for coherent optical communications. In such systems, a sub-THz carrier is generated by beating two optical tones in a high-speed photodiode, typically a uni-traveling-carrier photodiode (UTC-PD). Compared with purely electronic frequency multiplication schemes, optical heterodyning naturally provides a widely tunable carrier with excellent spectral purity while avoiding many of the spurious tones arising from higher-order nonlinearities [5], [14]. This is enabled by the square-law response of the photodiode,

*J. Dittmer and D. Pilori contributed equally to this work.

J. Dittmer, Md S. Mahmud, F. Gostner, L. Nolte, C. Koos and S. Randel are with the Institute of Photonics and Quantum Electronics (IPQ), Karlsruhe Institute of Technology (KIT), Germany.

D. Pilori is with the Department of Electronics and Telecommunications (DET), Politecnico di Torino, Italy.

A. Bhutani was with the Institute of Radio Frequency Engineering and Electronics (IHE), Karlsruhe Institute of Technology (KIT), Germany. In Jan 2026, she joined Infineon Technologies Austria AG, Siemenstrasse 2, 9500 Villach, Austria.

A.-C. Hilkert and T. Zwick are with the Institute of Radio Frequency Engineering and Electronics (IHE), Karlsruhe Institute of Technology (KIT), Germany.

A. Tessmann and S. Wagner are with the Fraunhofer Institute for Applied Solid State Physics IAF, Freiburg, Germany.

H. Li and L. Schmalen are with the Communications Engineering Lab (CEL), Karlsruhe Institute of Technology (KIT), Germany.

0000–0000/00$00.00 © 2026 IEEE

This work is licensed under a Creative Commons Attribution 4.0 License. For more information, see https://creativecommons.org/licenses/by/4.0/

This article has been accepted for publication in IEEE Transactions on Terahertz Science and Technology. This is the author's version which has not been fully edited and content may change prior to final publication. Citation information: DOI 10.1109/TTHZ.2026.3749414

TABLE I
COMPARISON OF HIGH-CAPACITY SUB-THZ WIRELESS TRANSMISSION DEMONSTRATIONS

Reference	Carrier	Distance	Data rate	Configuration	IEEE 802.15.3d
Chinni et al. [6]	280 GHz	0.5 m	100 Gbit/s*	16-QAM, single channel	Targeted Ch. 69
Dittmer et al. [7]	300 GHz	52 m	167 Gbit/s**	16-QAM, single carrier	Not reported
Fang et al. [8]	302 GHz	55 m	208 Gbit/s**	32-QAM, single carrier	Not reported
Maekawa et al. [9]	300 GHz	214 m	204 Gbit/s**	32-QAM, single carrier	Not reported
Zhang et al. [10]	300 GHz	100 m	1.034 Tbit/s**	Frequency/Polarization/Spatial multiplexing	Not reported
Abacıoğlu et al. [11]	280 GHz	0.25 m	100 Gbit/s*	16-QAM, single/dual channel	Targeted Ch. 66–69
Pilori et al. [12]	286 GHz	56 m	242 Gbit/s**	QPSK, single aperture, dual polarization	Targeted Ch. 69
Dittmer et al. [13]	287 GHz	56 m	405 Gbit/s**	16-QAM, single carrier, single aperture, dual polarization	Targeted Ch. 69
This work	**287 GHz**	**56 m**	**414.7 Gbit/s*** **	**16-QAM, single carrier, single aperture, dual polarization**	**Targeted Ch. 69**

* Line rate. No FEC applied ** Net data rate, with assumed FEC threshold *** Net data rate, with implemented FEC threshold

which inherently performs the mixing of the optical signals at the desired difference frequency. Furthermore, mature high-performance optical components, including narrow-linewidth lasers, high-bandwidth electro-optic modulators, and optical amplifiers, can be directly reused for sub-THz transmitter implementations.

These technological advances have enabled rapid progress in high-capacity laboratory wireless transmission systems. Optoelectronic transmitters have demonstrated line rates exceeding 200 Gbit/s over wireless distances beyond 50 m [7], [8]. Further capacity scaling has been achieved through the use of multiple frequency channels, spatial multiplexing, and parallel antenna apertures, resulting in aggregate transmission rates exceeding 1 Tbit/s [10]. At the receiver side, advances in integrated electronic front-end technology have enabled coherent receiver architectures with analog bandwidths sufficient to support symbol rates beyond 100 GBd [15] and wireless transmission distances exceeding 1 km [16]. Similar to coherent optical communication systems, coherent sub-THz receivers provide access to amplitude and phase information and therefore enable spectrally efficient higher-order modulation formats as well as advanced digital signal processing for carrier recovery, equalization, and impairment compensation.

The capacity of coherent sub-THz wireless links can be increased through three complementary approaches. First, improvements in transmitter output power and receiver sensitivity increase the available signal-to-noise ratio (SNR), enabling the use of higher-order modulation formats and consequently higher throughput. Second, spectral efficiency can be optimized through advanced coded-modulation techniques such as probabilistic constellation shaping (PCS) [17], which enables flexible rate adaptation and operation closer to the Shannon capacity limit [18]. PCS has become a key technology in modern coherent optical transmission systems and has been adopted, for example, in OpenROADM MSA specifications [19]. Although PCS has also been proposed for wireless communications [20], its practical benefits in sub-THz wireless systems remain insufficiently explored. In particular, hardware impairments such as phase noise, nonlinear distortions, and implementation penalties may reduce the theoretically achievable shaping gain, making the resulting performance strongly dependent on the employed forward-error correction (FEC) scheme. Third, transmission capacity can be increased through parallel communication channels using frequency, spatial, or polarization multiplexing. Among these approaches, polarization-division multiplexing (PDM) is particularly attractive because it approximately doubles spectral efficiency without increasing occupied bandwidth or requiring multiple independent propagation paths. Compared with spatial multiplexing, PDM significantly reduces antenna count, synchronization complexity, and alignment requirements while preserving the advantages of a single point-to-point wireless link.

Although polarization-multiplexed sub-THz transmission has recently attracted growing interest [10], [21], existing demonstrations have primarily focused on maximizing aggregate throughput rather than systematically investigating the trade-offs between modulation format, shaping gain, transmission robustness, and practical FEC operation. Furthermore, most reported experiments rely on pre-FEC metrics such as bit-error ratio (BER), error-vector magnitude (EVM), or generalized mutual information (GMI), whereas experimental validation using practical soft-decision FEC decoding has rarely been reported. As a result, the practical benefits of probabilistic shaping and dual-polarization transmission in coherent sub-THz wireless systems remain insufficiently quantified.

In our previous works, we reported coherent dual-polarization QPSK transmission over a 56-m single-aperture 287-GHz wireless link with a net data rate of 242 Gbit/s [12], and its extension to 16-QAM with net data rates above 400 Gbit/s [13]. These works primarily focused on selected operating points and relied on pre-FEC performance metrics. Building on the experimental platform introduced in [12], [13], this paper substantially extends the investigation to address the lack of systematic studies on the trade-off between modulation format, shaping gain, robustness and practical FEC operation identified above.

The new contributions of this paper are as follows. First, we systematically compare dual-polarization QPSK, uniform 16-QAM, and probabilistically shaped 16-QAM with entropies of 3.5 and 3.8 bit/symbol under identical experimental conditions over symbol rates from 30 to 64 GBd, considering signal-to-noise-and-distortion ratio (SNDR), NGMI, and achievable throughput. Second, we experimentally validate transmission using soft-decision SC-QC-LDPC decoding, selecting the code rate for each modulation format and symbol rate and thereby determining the post-FEC net throughput and required FEC overhead. Uniform 16-QAM reaches 414.7 Gbit/s, while PCS-16-QAM with 3.8 bit/symbol reaches 413.7 Gbit/s with a reduced FEC overhead of 16.7%, compared with 24% for

This work is licensed under a Creative Commons Attribution 4.0 License. For more information, see https://creativecommons.org/licenses/by/4.0/

This article has been accepted for publication in IEEE Transactions on Terahertz Science and Technology. This is the author's version which has not been fully edited and content may change prior to final publication. Citation information: DOI 10.1109/TTHZ.2026.3749414

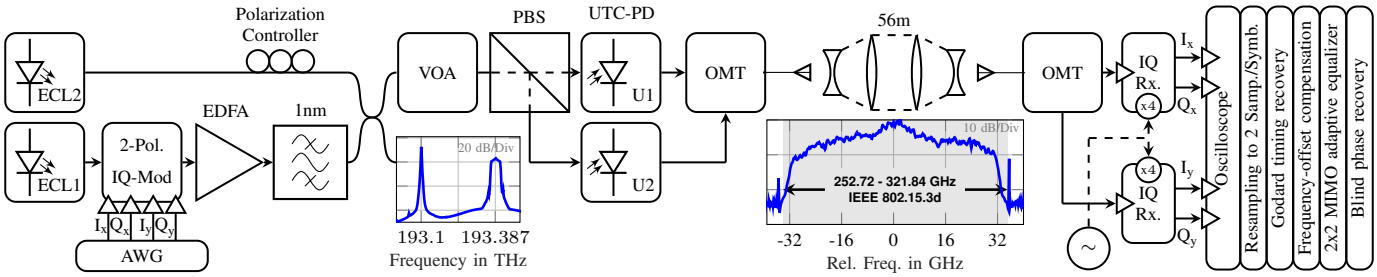

Fig. 1. Experimental setup of the dual-polarization point-to-point (P2P) sub-THz transmission system. The optoelectronic transmitter (left) generates a 287 GHz carrier through optical heterodyne downconversion of two optical tones (ECL1 and ECL2). ECL1 is modulated with independent dual-polarization IQ signals by an electro-optical IQ modulator. Subsequent to optical amplification, filtration, and power adjustment, the optical signal is converted to the electrical domain by beating in a UTC photodiode and radiated via the transmitting antenna. Subsequent to 56-m wireless propagation, the received sub-THz signal is captured by the receiving antenna and downconverted to baseband by an all-electronic coherent receiver (right), where orthogonal polarizations are separated, coherently down-converted, and detected for digital signal recovery. Insets illustrate the measured optical spectrum of the optical tone ECL2 and the modulated data around ECL1 (left) and the measured baseband spectrum after down-conversion (right). The IEEE 802.15.3d frequency allocation around 287 GHz is indicated for reference. (Extended from [13])

uniform 16-QAM. Finally, we compare the experimentally observed shaping gain with the ideal AWGN expectation and discuss the impact of residual hardware impairments.

To the best of our knowledge, this work reports the highest experimentally demonstrated net data rate of 414.7 Gbit/s in a single-aperture dual-polarization sub-THz wireless link, together with practical FEC validation. Furthermore, it provides a comprehensive experimental comparison of conventional and probabilistically shaped modulation formats in a coherent single-aperture dual-polarization sub-THz wireless system, thereby establishing practical design trade-offs among throughput, transmission robustness, and FEC implementation complexity. Table I summarizes high-capacity sub-THz wireless transmission demonstrations in the sub-THz range, including transmission distance, net data rate, and relationship to the IEEE 802.15.3d frequency allocation.

II. Experimental Setup and Digital Signal Processing

The experimental system is designed as a unified platform to investigate the impact of modulation format, symbol rate, and forward-error correction on the performance of high-capacity sub-THz wireless links. This section first introduces the dual-polarization 287-GHz point-to-point transmission setup, including the optoelectronic transmitter and the integrated coherent receiver. Afterwards, the corresponding digital signal processing algorithms used for synchronization, channel equalization, carrier recovery, performance estimation, and FEC decoding are presented.

A. Experimental Setup

As illustrated in Fig. 1, the point-to-point (P2P) sub-THz dual-polarization transmission link is based on a coherent dual-polarization optical transmitter combined with a dual-polarization all-electronic intradyne sub-THz receiver.

An external-cavity laser (ECL), denoted as ECL1, drives a dual-polarization $LiNbO_3$ IQ Mach-Zehnder modulator (MZM). The four electrical drive signals ($I_{x,y}$, $Q_{x,y}$) are generated by a 120-GSa/s arbitrary waveform generator (AWG) and pre-amplified by broadband 28 dB gain baseband amplifiers. Each tributary is shaped with a root-raised-cosine filter with a 5% spectral roll-off. The symbol rate is varied between 30 and 64 Gbaud. At the maximum symbol rate of 64 Gbaud, the transmitted spectrum, including the 5% roll-off, spans from 253.4 GHz to 320.6 GHz and remains entirely within the IEEE 802.15.3d band. After modulation, the optical signal is amplified by an erbium-doped fiber amplifier (EDFA), filtered with a 1-nm optical bandpass filter, and combined via a 3-dB coupler with a second ECL, denoted as ECL2, which is offset by 287 GHz and whose polarization is adjusted by a polarization controller. A variable optical attenuator (VOA) adjusts the launch power ahead of a polarization beam splitter (PBS).

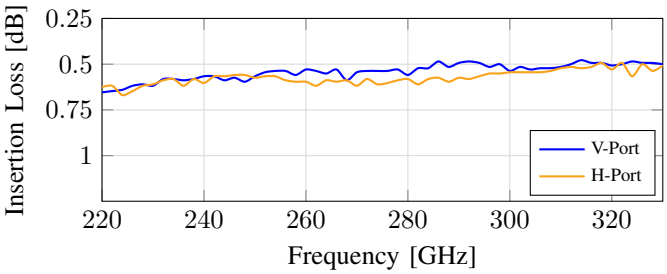

Fig. 2. Measured insertion loss of the WR-3.4 orthomode transducer (OMT) for the V-Port and H-Port over the 220–330 GHz band.

The two PBS outputs are individually downconverted by two broadband UTC photodiodes, where optical heterodyning between modulated ECL1 and ECL2 downconverts each polarization tributary to the sub-THz range of around 287 GHz. The resulting sub-THz signals are combined in a WR-3.4 orthomode transducer (OMT, OT034-MicroHarmonics) and radiated through a single dual-polarized circular horn antenna. The insertion loss over frequency for the vertical (V) and horizontal (H) polarization of the OMT is shown in Fig. 2.

The dual-polarization conical horn has an intrinsic gain of 26 dBi and a half-power beamwidth of around 9°, comparable to the single-polarization diagonal horn used in [22]. The employed horn is rotationally symmetric, with both polarizations sharing the same phase center, apart from mechanical tolerances. It is connected directly to the square common port of the OMT without an additional transition. Residual reflections and static delay differences between the two OMT arms are compensated by the 2×2 MIMO equalizer. The

This work is licensed under a Creative Commons Attribution 4.0 License. For more information, see https://creativecommons.org/licenses/by/4.0/

This article has been accepted for publication in IEEE Transactions on Terahertz Science and Technology. This is the author's version which has not been fully edited and content may change prior to final publication. Citation information: DOI 10.1109/TTHZ.2026.3749414

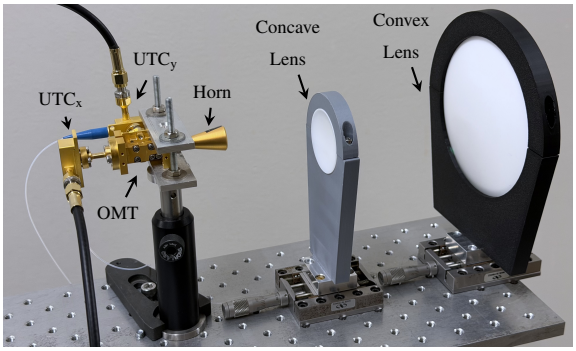

Fig. 3. Dual-polarization optoelectronic transmitter based on two uni-traveling carrier (UTC$_x$ and UTC$_y$) photodiodes combined with an orthomode transducer (OMT) and a dual-polarization horn antenna with integrated, cascaded polytetrafluoroethylene (PTFE) lenses (concave/convex) (Adapted from [13]).

antenna gain is enhanced by a cascaded concave-convex PTFE lens system. The lens system and its mechanical spacing are identical to those in [22]. The horn-to-concave-lens distance is 108.3 mm and the concave-to-convex-lens spacing is 127.1 mm, resulting in a total distance of 235.4 mm. The overall gain of approximately 51.1 dBi and the full-width-at-half-maximum beam divergence of 0.57° reported in [22] are used as reference values for both orthogonal E- and H- planes and are reproduced by the same Gaussian-beam model. The transmitter, consisting of the two UTC photodiodes and the cascaded lenses, is shown in Fig. 3.

At the receiver, an identical cascaded-lens horn antenna collects the signal, and a second OMT separates the two received polarizations, which are processed by two synchronized intradyne, ultra-broadband, all-electronic receiver chains. The receiver lens antenna with electronic mixers is shown in Fig. 4. The novel WR-3.4 waveguide receiver modules are based on

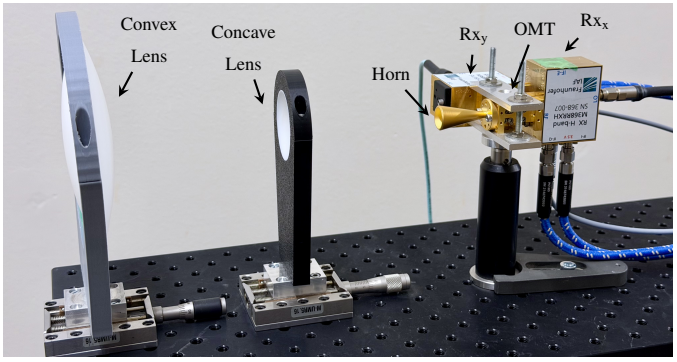

Fig. 4. Dual-polarization electronic receiver based on two electronic 35 nm mHEMT subharmonic mixers (Rx$_x$/Rx$_y$) combined with an orthomode transducer (OMT) and a dual-polarization horn antenna with integrated, cascaded polytetrafluoroethylene (PTFE) lenses (concave/convex) (Adapted from [13]).

a fully integrated, multifunctional front-end MMIC fabricated in Fraunhofer IAF's state-of-the-art 35-nm metamorphic high-electron-mobility transistor (mHEMT) technology [23]. The present chip represents the next generation of the 300-GHz communication receiver reported in [24], and advances that design primarily at the architectural level. In the earlier work, the subharmonic 100-GHz LO was generated externally by a broadband $\times 12$ multiplier MMIC driven from an 8.333-GHz X-band reference, tripled to 300 GHz on-chip, and applied to a fundamental mixer. The receiver employed here instead performs a fourfold electrical LO multiplication on-chip and adopts a second-harmonic mixing scheme, which relaxes the on-chip LO frequency requirements and simplifies the reference generation. A microscope image of the complete receiver chip is shown in Fig. 5 [23].

Each receiver is driven by a common external reference at 35.875 GHz, which serves as the LO tone for the entire chain. On-chip, this reference undergoes a fourfold electrical multiplication ($\times 4$), followed by an amplifier that boosts the multiplied signal to the power level required to pump the mixer. Down-conversion is then performed by a second-harmonic sub-THz IQ mixer, providing direct access to both the I and Q components and thus enabling coherent recovery of amplitude and phase, while retaining the DC-coupled quadrature IF channels required for zero-IF operation.

The choice of a second-harmonic mixer over the fundamentally pumped topology of [24] is motivated primarily by the improvement it brings to signal reception. Because the physical LO operates at half the RF frequency, LO-to-RF leakage falls outside the RF band and the DC offset arising from LO self-mixing, which is a primary impairment of fundamental direct-conversion receivers that distorts the signal constellation and degrades the effective SNR, is intrinsically suppressed. The result is a cleaner baseband and a higher signal linearity, which directly translates into greater link margin and support for higher-order modulation formats and thus higher spectral efficiency at a given link budget.

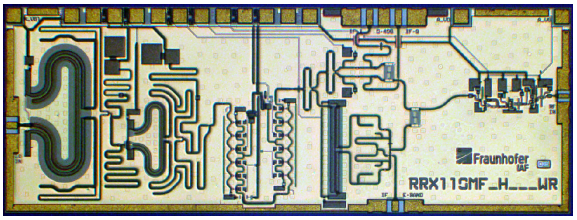

Fig. 5. Fully integrated 35 nm mHEMT receiver MMIC including a three-stage low-noise amplifier (LNA) followed by the second harmonic mixer, providing 0 dB conversion gain and an approximately 7 dB noise figure across 220–330 GHz. (Adapted from [23])

Ahead of the mixer, the incoming RF signal is amplified by a three-stage low-noise amplifier (LNA) exhibiting a small-signal gain of 28 dB, resulting in an overall conversion gain of 0 dB, and a noise figure of approximately 7 dB across an operating bandwidth from 220 GHz to 330 GHz. This represents a significant bandwidth extension over the receiver of [24], whose four-stage LNA provided a 25-dB gain and a 6.5-dB noise figure over a narrower RF range of 292 to 314 GHz. By providing substantial gain prior to down-conversion, the LNA suppresses the noise contribution of the mixer and sets the low overall receiver noise figure, making the module a compact and versatile building block for next-generation sub-THz communication and sensing systems.

The four receiver outputs are further amplified by two baseband amplifiers, each having a small-signal gain of 11 dB, and digitized by a four-channel real-time oscilloscope with 80-GHz analog bandwidth and a sampling rate of 256 GSa/s.

This work is licensed under a Creative Commons Attribution 4.0 License. For more information, see https://creativecommons.org/licenses/by/4.0/

This article has been accepted for publication in IEEE Transactions on Terahertz Science and Technology. This is the author's version which has not been fully edited and content may change prior to final publication. Citation information: DOI 10.1109/TTHZ.2026.3749414

B. Digital Signal Processing

The transmit sequences were generated using both QPSK and 16-QAM constellations. The 16-QAM constellation was optionally probabilistically shaped (PCS) using two Maxwell–Boltzmann distributions with target entropies of 3.5 and 3.8 bit/symbol. Although this distribution is theoretically optimal only for the Gaussian channel [25], it has been widely adopted for nonlinear optical communication channels [26]. PCS was implemented assuming an ideal constant-composition distribution matcher (CCDM) [27], with a blocklength equal to the length of the transmit sequence. The theoretical NGMI of the three 16-QAM constellations is shown in Fig. 6. The values were obtained using Gauss–Hermite quadrature [28] under the assumption of a purely Gaussian channel. Compared with uniform 16-QAM, PCS achieves the same NGMI at a lower SNR, albeit with reduced throughput, thereby providing finer-grained data-rate flexibility than conventional QAM constellations.

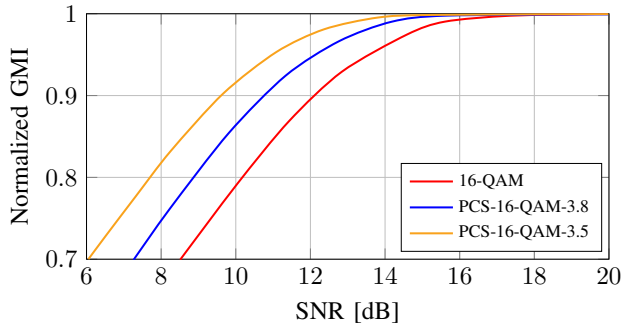

Fig. 6. Theoretical normalized generalized mutual information for uniform 16-QAM, and 16-QAM with two different shaping factors, achieving an entropy of 3.5 and 3.8 bit/symbol. The NGMI is computed assuming an AWGN channel using Gauss-Hermite quadrature.

The receiver DSP is performed offline, and closely follows the standard DSP of an optical coherent receiver [29]. The recorded waveforms are first resampled to 2 samples per symbol, followed by blind timing recovery using the Godard algorithm [30]. A periodogram-based coarse frequency-offset estimator is then employed to compensate for the residual frequency mismatch between the transmitter and receiver local oscillators.

After coarse frequency synchronization, the two polarization tributaries are jointly processed by a 2×2 multiple-input multiple-output (MIMO) adaptive equalizer to compensate for polarization mixing in the optical channel, and residual linear impairments introduced by the optical transmitter, wireless channel, and receiver front-end. Different equalizer adaptation strategies are adopted depending on the modulation format.

For QPSK transmission, a 42-tap fully-blind constant-modulus algorithm (CMA) equalizer [31] is employed. Carrier phase recovery is subsequently performed using the fourth-power (Viterbi–Viterbi) algorithm [32]. For uniform and probabilistically shaped 16-QAM, the equalizer was instead based on the least-mean-square (LMS) criterion. Carrier phase recovery is then performed by blind phase search (BPS) using a phase resolution of 3° [33], followed by a maximum-likelihood stage with an averaging length of 100 symbols [34].

Following carrier recovery, the received symbols are compared with the transmitted sequences to evaluate the transmission performance. First, we compute the SNDR for all modulation formats. For QPSK, we also evaluate the pre-FEC bit-error ratio (BER) assuming hard-decision detection.

Instead, for 16-QAM, bit-wise log-likelihood ratios (LLRs) are calculated assuming bit-interleaved coded modulation (BICM) [35] over an additive white Gaussian noise (AWGN) channel [28]. The LLRs are used to evaluate the NGMI [36] with a Monte-Carlo method, which accurately predicts the achievable performance of BICM [28]. Finally, the received data are also decoded with a set of quasi-cyclic low-density parity-check (SC-QC-LDPC) codes [37] at different rates to compute the achievable post-FEC throughput.

III. Experimental Results

The proposed dual-polarization 287-GHz wireless link was experimentally evaluated over a 56-m line-of-sight indoor link along a long hallway.

A. Optical Power Optimization

Before comparing different modulation formats, the transmitter operating point was optimized by varying the optical launch power at the output of the variable optical attenuator (VOA). Figure 7 reports the measured performance for dual-polarization QPSK at 30 GBd.

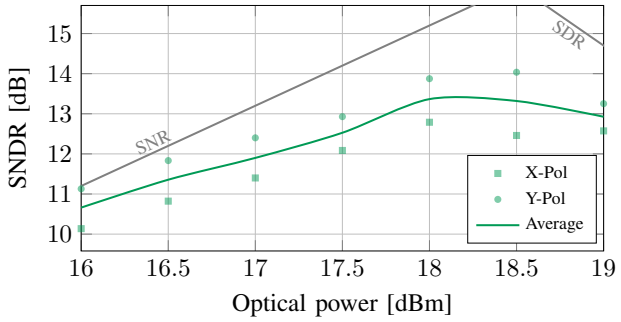

Fig. 7. Signal-to-noise and distortion (SNDR) as a function of transmit optical power for QPSK with 30 GBd. SNR (2 dB/dB) and SDR (-3 dB/dB) scaling are shown in gray.

As the optical power increases, the received SNDR initially improves because the generated sub-THz power increases. Beyond approximately 18.5 dBm, however, nonlinear distortion, attributed to the UTC photodiodes and the receiver front-end, increasingly offsets the SNR gain, resulting in a gradual performance degradation. Consequently, an optical launch power around 18.5 dBm was selected for all subsequent experiments. To quantify the contributions, the SNDR in Fig. 7 was decomposed as $1/\mathrm{SNDR} = 1/\mathrm{SNR} + 1/\mathrm{SDR}$. The thermal noise limited SNR was assumed to increase quadratically with the optical power (2 dB/dB, since both optical tones are attenuated by the VOA), while the SDR was assumed to decrease by 2–4 dB/dB, consistent with effective second- to third-order nonlinear distortion of the heterodyne signal. At 18.5 dBm, this yields an SNR and SDR of approximately 16.2 dB, i.e., noise and distortion contribute

This work is licensed under a Creative Commons Attribution 4.0 License. For more information, see https://creativecommons.org/licenses/by/4.0/

This article has been accepted for publication in IEEE Transactions on Terahertz Science and Technology. This is the author's version which has not been fully edited and content may change prior to final publication. Citation information: DOI 10.1109/TTHZ.2026.3749414

comparably and distortion reduces the SNDR by about 3 dB. The decomposition depends on the assumed power scaling and does not separate the contributions of the UTC photodiodes and the receiver, whose saturation characteristics were not measured individually.

A residual performance difference of approximately 1 dB is observed between the two polarization tributaries. This imbalance remains nearly constant over the investigated operating range and is mainly attributed to residual polarization-dependent loss of the transmitter setup.

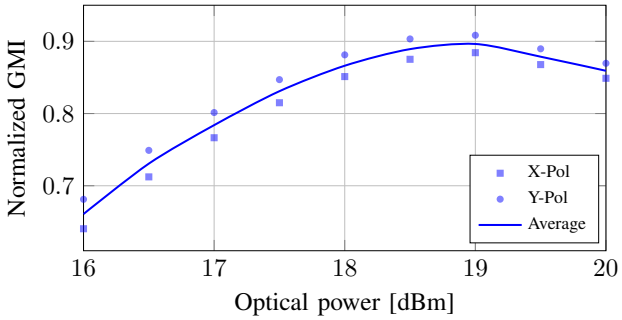

Fig. 8. Normalized generalized mutual information (NGMI) as function of transmit optical power for PCS-16-QAM at 64 GBd.

The optimum launch power is largely independent of the employed modulation format. Figure 8 shows the measured NGMI for PCS-16-QAM at 64 GBd as a function of optical launch power. In agreement with the QPSK measurements of Fig. 7, the performance first improves with increasing launch power owing to the higher generated sub-THz output power. Once the optical launch power exceeds approximately 19 dBm, nonlinear distortions in the optoelectronic transmitter and receiver front-end outweigh the SNR improvement, leading to a reduction in NGMI. The maximum NGMI is therefore obtained for launch powers between 18 and 19 dBm, confirming that this operating point provides the best trade-off between noise efficiency and nonlinear distortion for both modulation formats.

B. Increasing the Symbol Rate

Using the optimized operating point, the symbol rate was increased from 30 to 64 GBd. Figure 9 shows the measured SNDR for dual-polarization QPSK, 16-QAM, and probabilistically shaped 16-QAM.

The average SNDR decreases almost linearly from approximately 14.6 dB at 30 GBd to approximately 11.5 dB at 64 GBd, mainly because increasing bandwidth exposes the transmission to a larger amount of noise and analog frequency-response limitations of the transmitter and receiver chain. Nevertheless, both polarization channels exhibit nearly identical behavior over the entire investigated symbol-rate range, confirming the good balance of the dual-polarization transmitter and receiver architecture.

Fig. 10 shows the carrier phase estimated by the receiver DSP at 64 GBd. After coarse frequency-offset compensation, the residual offset is below 55 kHz. The equivalent combined linewidth of the transmitter and receiver, including the heterodyne beat of the two ECLs and the receiver LO chain, is

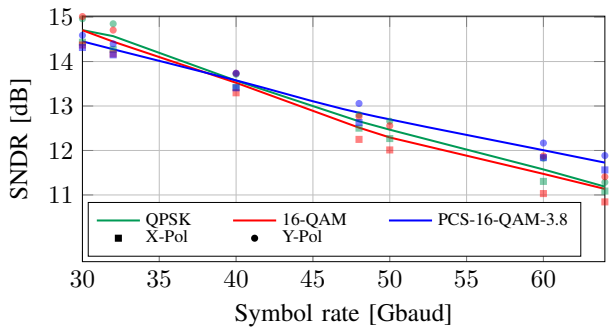

Fig. 9. Measured signal-to-noise and distortion ratio (SNDR) as a function of symbol rate for QPSK, 16-QAM, and PCS-16-QAM with an entropy of 3.8 bit/symbol.

approximately 20–50 kHz for all formats. The resulting phase-noise-limited SNR exceeds 34 dB, well above the measured SNDR of 11–15 dB. The phase noise is therefore not a limiting factor for the demonstrated rates.

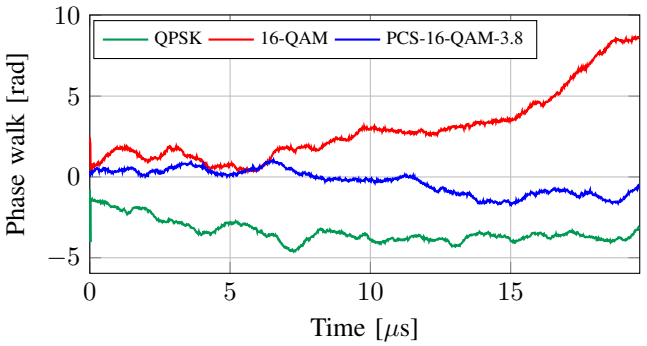

Fig. 10. Carrier phase estimated by the receiver DSP at 64 GBd (residual frequency offset and its linear drift removed).

At the highest symbol rate, the BER for QPSK is approximately 10^{-4}, which is below the threshold for the IEEE-standardized KP4 FEC [38] ($\sim 2 \times 10^{-4}$). Therefore, with QPSK the system transmits a net throughput of approximately 241.9 Gbit/s using a simple and blind DSP, followed by a low-latency hard-decision FEC.

C. Normalized GMI

The achievable transmission performance for higher-order modulation formats is then evaluated through the NGMI. After computing the GMI from the LLRs with a Monte-Carlo method [28], the NGMI is computed for uniform 16-QAM by

$$\mathrm{NGMI}_{\text{16-QAM}} = \mathrm{GMI}/4\,. \tag{1}$$

For QPSK, NGMI is analogously computed as $\mathrm{GMI}/2$. With PCS-16-QAM, instead, it is computed as

$$\mathrm{NGMI}_{\text{PCS-16-QAM}} = 1 - (\mathcal{H}(X) - \mathrm{GMI})/4 \tag{2}$$

where $\mathcal{H}(X)$ is the constellation entropy, i.e., 3.8 and 3.5 bit/symbol. Even though each point has a different net throughput, the NGMI allows a straightforward comparison among different constellations for the same soft-decision FEC. To ease the comparison, the dashed line corresponds to a conventional soft-decision FEC threshold with a 20% overhead [37] and an additional 0.95% rate loss. Nevertheless, the

This work is licensed under a Creative Commons Attribution 4.0 License. For more information, see https://creativecommons.org/licenses/by/4.0/

This article has been accepted for publication in IEEE Transactions on Terahertz Science and Technology. This is the author's version which has not been fully edited and content may change prior to final publication. Citation information: DOI 10.1109/TTHZ.2026.3749414

exact performance with real FEC codes will be shown in the following section.

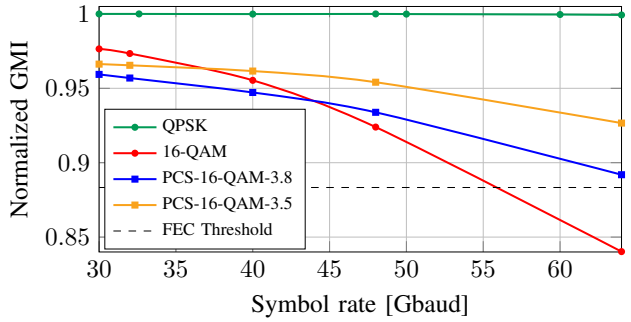

Fig. 11. Polarization-averaged normalized generalized mutual information (NGMI) as a function of symbol rate for QPSK, 16-QAM, PCS-16-QAM-3.8, and PCS-16-QAM-3.5. The dashed line indicates the NGMI threshold of 0.883 corresponding to a 20% FEC code with an additional 0.95% rate loss.

At low symbol rates, all investigated modulation formats achieve a high NGMI, indicating reliable transmission with a substantial margin to the FEC threshold. As the symbol rate increases, however, the NGMI gradually decreases owing to the reduced received SNR and the increased impact of hardware impairments. This degradation is most pronounced for uniform 16-QAM, which approaches the FEC threshold at approximately 55 GBd. In contrast, PCS-16-QAM maintains a higher NGMI at elevated symbol rates because its nonuniform probability distribution provides improved power efficiency and robustness to noise, albeit at the cost of reduced net throughput. Among the investigated shaping distributions, PCS-16-QAM with an entropy of 3.8 bit/symbol provides the best compromise between achievable throughput and decoding margin, whereas the 3.5 bit/symbol distribution offers the highest robustness at the expense of spectral efficiency.

D. Achievable Throughput

The corresponding net (i.e. post-FEC) throughput is summarized in Fig. 12. Dual-polarization QPSK provides the most robust transmission, reaching a net throughput of approximately 241.9 Gbit/s at 64 GBd when combined with a fixed hard-decision KP4 FEC (5.84% overhead). For 16-QAM (with and without PCS), for each point, we tested a set of different soft-decision SC-QC-LDPC codes with different rates, choosing the highest-rate code that gave error-free transmission [37].

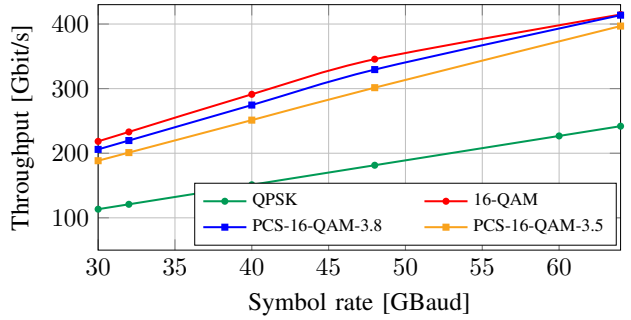

Fig. 12. Throughput as a function of symbol rate using the optimal FEC code rate for each symbol rate and modulation format.

For PCS, the net throughput was computed assuming the use of the probability amplitude shaping (PAS) architecture [17]. The results at the highest symbol rate of 64 GBd are also reported in Table II. Both uniform 16-QAM and PCS-16-QAM-3.8 achieve approximately the same net data rate, but PCS achieves it with a significantly smaller FEC overhead (from 24% to 16.7%). PCS-16-QAM-3.5 achieves instead a slightly smaller throughput, but with an even simpler FEC implementation with 11.4% overhead. Consequently, although PCS slightly reduces the maximum achievable throughput, it consistently increases the decoding margin for a fixed FEC overhead.

TABLE II
SUMMARY OF RESULTS AT 64 GBAUD

Modulation	FEC overhead (%)	Net throughput (Gbit/s)	NGMI
QPSK	5.84	241.9	> 0.99
PCS-16-QAM-3.5	11.4	396.9	0.93
PCS-16-QAM-3.8	16.7	413.7	0.89
16-QAM	24.0	414.7	0.84

The experimentally observed shaping gain is somewhat smaller than predicted for an ideal AWGN channel, indicating that residual nonlinear distortion of the transmitter and receiver affects probabilistically shaped constellations more strongly than uniform 16-QAM. Future work will further investigate this aspect by tailoring PCS [26], [39] to the nonlinear behavior of the wireless THz channel.

IV. CONCLUSION

We have experimentally demonstrated a coherent single-aperture dual-polarization wireless transmission system operating at 287 GHz over a 56-m point-to-point link and performed a comprehensive comparison of QPSK, uniform 16-QAM, and probabilistically shaped 16-QAM under identical experimental conditions. By combining photonic carrier generation with integrated ultra-broadband coherent receiver front-ends fabricated in 35-nm mHEMT technology, the proposed architecture enables polarization-division multiplexing using a single dual-polarized antenna aperture at each end of the wireless link, thereby doubling the spectral efficiency without requiring parallel propagation paths.

The experimental results quantify the trade-offs between transmission robustness and achievable throughput. Dual-polarization QPSK provides the highest robustness, maintaining an average SNDR above 11 dB across symbol rates from 30 to 64 GBd and supporting low-complexity hard-decision FEC. Uniform 16-QAM achieves the highest throughput, reaching a net data rate of 414.7 Gbit/s at 64 GBd after practical SC-QC-LDPC decoding.

Probabilistically shaped 16-QAM, while providing a slightly lower maximum throughput, consistently increases the NGMI and therefore the decoding margin, enabling more flexible adaptation of the transmission rate to the available channel quality. These results highlight the complementary roles of conventional and shaped modulation formats for future adaptive sub-THz wireless systems.

This work is licensed under a Creative Commons Attribution 4.0 License. For more information, see https://creativecommons.org/licenses/by/4.0/

This article has been accepted for publication in IEEE Transactions on Terahertz Science and Technology. This is the author's version which has not been fully edited and content may change prior to final publication. Citation information: DOI 10.1109/TTHZ.2026.3749414

Overall, the presented work demonstrates that coherent dual-polarization transmission is a viable approach toward terabit-class wireless links within the IEEE 802.15.3d frequency allocation. Beyond reporting the highest experimentally demonstrated net data rate for a single-aperture dual-polarization sub-THz wireless link, the paper provides practical design guidelines for selecting modulation formats and coding schemes according to the desired balance between throughput, robustness, and implementation complexity. Future work will investigate longer transmission distances, optimized constellation shaping, and real-time DSP toward deployable ultra-high-capacity sub-THz wireless fronthaul, backhaul, and data-center interconnects.

ACKNOWLEDGMENT

The authors would like to thank G. Bosco and A. M. Rosa Brusin from Politecnico di Torino for useful discussions.

This work is financially supported by the German Federal Ministry of Research, Technology and Space (BMFTR) within the projects *Open6GHub* (16KISK010) and *Open6GHub+* (16KIS2405) as well as by the Horizon Europe research and innovation programme within the project *X-TREME 6G* (101192681) and by the Department of Electronics and Telecommunications (DET) of Politecnico di Torino (*Incentivazione Dipartimentale – Azione A1.2*).

Portions of this manuscript were prepared with the assistance of ChatGPT Edu (OpenAI) for language refinement and early drafting support. The authors reviewed, verified, and edited all AI-generated content and take full responsibility for the final manuscript.

REFERENCES

[1] C.-X. Wang, X. You, X. Gao, X. Zhu, Z. Li, C. Zhang, H. Wang, Y. Huang, Y. Chen, H. Haas, J. S. Thompson, E. G. Larsson, M. D. Renzo, W. Tong, P. Zhu, X. Shen, H. V. Poor, and L. Hanzo, "On the road to 6G: Visions, requirements, key technologies, and testbeds," *IEEE Commun. Surveys Tuts.*, vol. 25, no. 2, pp. 905–974, 2023.

[2] V. Petrov, T. Kurner, and I. Hosako, "IEEE 802.15.3d: First standardization efforts for sub-terahertz band communications toward 6G," *IEEE Commun. Mag.*, vol. 58, no. 11, pp. 28–33, 2020.

[3] I. Atzeni, G. R. d. L. Tejerina, R. Berkvens, H. Chen, J.-M. Conrat, M. F. D. Guzman, C. Desset, M. Dörpinghaus, H. Farhadi, G. Fettweis, F. Gast, H. Halbauer, R. Halili, K. Haneda, I. Harjula, B. Jahan, R. Khayatzadeh, P. Kyösti, R. Legouable, A. Lehti, D. Marasinghe, L. H. Nguyen, S. Saleh, K. Senparlak, N. Tervo, O. Tervo, H. Wymeersch, B. Xu, and P. Zhang, "Sub-THz communications: Perspective and results from the Hexa-X-II project," *IEEE Open J. Commun. Soc.*, vol. 6, pp. 7495–7540, 2025.

[4] M. Tonouchi, "Cutting-edge terahertz technology," *Nature photonics*, vol. 1, no. 2, pp. 97–105, 2007.

[5] T. Nagatsuma, G. Ducournau, and C. C. Renaud, "Advances in terahertz communications accelerated by photonics," *Nature Photonics*, vol. 10, no. 6, pp. 371–379, 2016.

[6] V. Chinni, P. Latzel, M. Zégaoui, C. Coinon, X. Wallart, E. Peytavit, J. Lampin, K. Engenhardt, P. Szriftgiser, M. Zaknoune, and G. Ducournau, "Single-channel 100 Gbit/s transmission using III–V UTC-PDs for future IEEE 802.15.3d wireless links in the 300 GHz band," *Electronics Letters*, vol. 54, no. 10, pp. 638–640, 2018.

[7] J. Dittmer, J. Tebart, C. Füullner, C. Koos, A. Stöhr, and S. Randel, "200 gbit/s wireless thz transmission over 52m using optoelectronic signal generation," in *2023 53rd European Microwave Conference (EuMC)*, 2023, pp. 134–137.

[8] D. Fang, H. Peng, Y. Chen, J. Dittmer, A. Tessmann, S. Wagner, P. Matalla, D. Drayss, G. Lihachev, A. Voloshin, S. T. Skacel, M. Lauermann, I. Kallfass, T. Zwick, W. Freude, T. J. Kippenberg, S. Randel, and C. Koos, "Wireless THz communications at 250 Gbit/s using self-injection-locked Kerr soliton microcombs as photonic-electronic oscillators at the transmitter and receiver," in *Proc. 50th Eur. Conf. Opt. Commun. (ECOC)*, 2024, pp. 558–561.

[9] K. Maekawa, T. Yoshioka, T. Nakashita, T. Ohara, and T. Nagatsuma, "Single-carrier 220-Gbit/s sub-THz wireless transmission over 214 m using a photonics-based system," *Opt. Lett.*, vol. 49, no. 16, pp. 4666–4668, Aug 2024. [Online]. Available: https://opg.optica.org/ol/abstract.cfm?URI=ol-49-16-4666

[10] H. Zhang, Z. Yang, Z. Lyu, H. Yang, L. Zhang, O. Ozolins, X. Pang, X. Zhang, and X. Yu, "300 GHz photonic-wireless transmission with aggregated 1.034 Tbit/s data rate over 100 m wireless distance," in *Proc. Opt. Fiber Commun. Conf. (OFC)*, 2024, p. M2F.1.

[11] E. Abacıoğlu, A. S. Mohammed, J. Tebart, M. Grzeslo, T. Neerfeld, J. L. F. Estévez, P. Szriftgiser, G. Ducournau, and A. Stöhr, "100 Gbit/s and beyond IEEE 802.15.3d channelization compatible THz communications enabled by a broadband MUTC photodiode," *IEEE Transactions on Terahertz Science and Technology*, vol. 15, no. 3, pp. 389–399, 2025.

[12] D. Pilori, J. Dittmer, S. Wagner, A. Tessmann, and S. Randel, "Photonic-generated 256-gbit/s dual-polarization 286-ghz wireless transmission over 56 m," in *Proceedings of the 2026 Italian Conference on Optics and Photonics (ICOP)*. L'Aquila, Italy: IEEE, Jun. 2026.

[13] J. Dittmer, D. Pilori, A. Bhutani, F. Beuthan, J. Seidel, Y. Mezger, A. Tessmann, S. Wagner, L. Nolte, H. Li, W. Freude, C. Koos, T. Zwick, L. Schmalen, and S. Randel, "400-gbit/s net transmission over a 56-m single-carrier and single-aperture dual-polarization sub-thz link," in *Proceedings of the European Conference on Optical Communication (ECOC)*. Málaga, Spain: IEEE, Sep. 2026.

[14] S. Koenig, D. Lopez-Diaz, J. Antes, F. Boes, R. Henneberger, A. Leuther, A. Tessmann, R. Schmogrow, D. Hillerkuss, R. Palmer *et al.*, "Wireless sub-THz communication system with high data rate," *Nat. Photonics*, vol. 7, no. 12, pp. 977–981, 2013.

[15] J. Long, J. Yu, X. Yang, Y. Wu, Y. Wang, Q. Zhang, Y. Chen, W. Li, K. Wang, W. Zhou, Y. Wei, F. Zhao, J. Yu, C. Jiang, S. Deng, and N. Xu, "Demonstration of 104-GBaud/λ digital subcarrier multiplexing 317-GHz THz signal wireless delivery based on photonics-aided technologies," in *Proc. Opt. Fiber Commun. Conf. (OFC)*. Optica Publishing Group, 2026, p. M4H.1.

[16] W. Li, J. Yu, X. Zhao, X. Lu, Y. Zhou, J. Chen, K. Wang, W. Zhou, K. Li, M. Zhu, J. Zhang, J. Yu, and F. Zhao, "Field trials of photonics 312 ghz terahertz-wave signals transmission over 3 km wireless distance," in *Optical Fiber Communication Conference (OFC) 2026*. Optica Publishing Group, 2026, p. M4H.7. [Online]. Available: https://opg.optica.org/abstract.cfm?URI=OFC-2026-M4H.7

[17] G. Böcherer, F. Steiner, and P. Schulte, "Bandwidth efficient and rate-matched low-density parity-check coded modulation," *IEEE Trans. Commun.*, vol. 63, no. 12, pp. 4651–4665, 2015.

[18] D. Pilori, L. Bertignono, A. Nespola, F. Forghieri, and G. Bosco, "Comparison of probabilistically shaped 64qam with lower cardinality uniform constellations in long-haul optical systems," *Journal of Lightwave Technology*, vol. 36, no. 2, pp. 501–509, 2018.

[19] M. Birk, O. Renais, G. Lambert, C. Betoule, G. Thouenon, A. Triki, D. Bhardwaj, S. Vachhani, N. Padi, and S. Tse, "The openroadm initiative [invited]," *Journal of Optical Communications and Networking*, vol. 12, no. 6, pp. C58–C67, 2020.

[20] J. Fang, Q. Li, C. Chen, A. Gurevitz, and Y. Yoffe, "Probabilistic shaping for wi-fi 8," *IEEE Journal on Selected Areas in Communications*, vol. 43, no. 11, pp. 3708–3721, 2025.

[21] C. Castro, R. Elschner, T. Merkle, C. Schubert, and R. Freund, "Experimental demonstrations of high-capacity THz-wireless transmission systems for beyond 5G," *IEEE Commun. Mag.*, vol. 58, no. 11, pp. 41–47, 2020.

[22] J. Dittmer, A. Bhutani, F. Beuthan, J. Krimmer, T. Zwick, C. Koos, and S. Randel, "Design, modeling, and characterization of a cascaded-lens antenna for 220–330 GHz with 51.1 dBi gain," *IEEE Open J. Antennas Propag.*, 2026.

[23] R. Weber *et al.*, "A 220 to 330 GHz dual-IF receiver-chip in 35-nm mHEMT technology," in *Proceedings of the European Microwave Week (EuMW 2026)*, London, United Kingdom, 2026.

[24] I. Kallfass, P. Harati, I. Dan, J. Antes, F. Boes, S. Rey, T. Merkle, S. Wagner, H. Massler, A. Tessmann, and A. Leuther, "MMIC chipset for 300 GHz indoor wireless communication," in *2015 IEEE International*

This work is licensed under a Creative Commons Attribution 4.0 License. For more information, see https://creativecommons.org/licenses/by/4.0/

This article has been accepted for publication in IEEE Transactions on Terahertz Science and Technology. This is the author's version which has not been fully edited and content may change prior to final publication. Citation information: DOI 10.1109/TTHZ.2026.3749414

Conference on Microwaves, Communications, Antennas and Electronic Systems (COMCAS), 2015, pp. 1–4.
[25] F. Kschischang and S. Pasupathy, "Optimal nonuniform signaling for gaussian channels," *IEEE Transactions on Information Theory*, vol. 39, no. 3, pp. 913–929, 1993.
[26] S. Civelli, E. Forestieri, and M. Secondini, "Probabilistic shaping methods for linear and nonlinear channels," in *2023 Optical Fiber Communications Conference and Exhibition (OFC)*, 2023, pp. 1–3.
[27] P. Schulte and G. Böcherer, "Constant composition distribution matching," *IEEE Transactions on Information Theory*, vol. 62, no. 1, pp. 430–434, 2016.
[28] A. Alvarado, T. Fehenberger, B. Chen, and F. M. J. Willems, "Achievable information rates for fiber optics: Applications and computations," *J. Lightw. Technol.*, vol. 36, no. 2, pp. 424–439, 2018.
[29] S. J. Savory, "Digital coherent optical receivers: Algorithms and subsystems," *IEEE Journal of Selected Topics in Quantum Electronics*, vol. 16, no. 5, pp. 1164–1179, 2010.
[30] D. Godard, "Passband timing recovery in an all-digital modem receiver," *IEEE Transactions on Communications*, vol. 26, no. 5, pp. 517–523, 1978.
[31] ——, "Self-recovering equalization and carrier tracking in two-dimensional data communication systems," *IEEE Transactions on Communications*, vol. 28, no. 11, pp. 1867–1875, 1980.
[32] A. J. Viterbi and A. M. Viterbi, "Nonlinear estimation of psk-modulated carrier phase with application to burst digital transmission," *IEEE Transactions on Information Theory*, vol. 29, no. 4, pp. 543–551, 1983.
[33] T. Pfau, S. Hoffmann, and R. Noe, "Hardware-efficient coherent digital receiver concept with feedforward carrier recovery for m-QAM constellations," *J. Lightw. Technol.*, vol. 27, no. 8, pp. 989–999, 2009.
[34] X. Zhou, "An improved feed-forward carrier recovery algorithm for coherent receivers with M-QAM modulation format," *IEEE Photonics Technology Letters*, vol. 22, no. 14, pp. 1051–1053, 2010.
[35] G. Caire, G. Taricco, and E. Biglieri, "Bit-interleaved coded modulation," *IEEE Transactions on Information Theory*, vol. 44, no. 3, pp. 927–946, 1998.
[36] J. Cho, L. Schmalen, and P. J. Winzer, "Normalized generalized mutual information as a forward error correction threshold for probabilistically shaped QAM," in *Proc. Eur. Conf. Opt. Commun. (ECOC)*, 2017.
[37] A. Ghazisaeidi, L. Schmalen, I. F. de Jauregui Ruiz, P. Tran, C. Simonneau, P. Brindel, and G. Charlet, "Transoceanic transmission systems using adaptive multirate FECs," *J. Lightw. Technol.*, vol. 33, no. 7, pp. 1479–1487, 2015.
[38] "Ieee standard for ethernet," *IEEE Std 802.3-2022 (Revision of IEEE Std 802.3-2018)*, pp. 1–7025, 2022.
[39] E. M. Liang and J. M. Kahn, "Probabilistic shaping distributions for optical communications," *Journal of Lightwave Technology*, vol. 43, no. 4, pp. 1501–1524, 2025.



Joel Dittmer received the B.Sc. and M.Sc. degrees in Electrical Engineering from the Karlsruhe Institute of Technology (KIT), Karlsruhe, Germany, in 2020 and 2022, respectively. In 2023, he joined the Institute of Photonics and Quantum Electronics (IPQ) at KIT as a Research Assistant. His research focuses on terahertz communication systems based on optoelectronic and electronic signal generation, including terahertz system and package design as well as high-data-rate digital signal processing.



Dario Pilori (Senior Member, IEEE) received the B.Sc. and M.Sc. degrees (cum laude) in Telecommunications Engineering from Politecnico di Milano, Italy, in 2012 and 2015, respectively, and the Ph.D. degree (cum laude) in Electrical, Electronics and Communications Engineering from Politecnico di Torino, Italy, in 2019. From 2013 to 2015, he was an International Research Intern with Alcatel-Lucent Bell Labs, Holmdel, NJ, USA. He was a Visiting Researcher at the Institute of Photonics and Quantum Electronics (IPQ), Karlsruhe Institute of Technology (KIT), Germany, in 2018 and 2025. From 2019 to 2023, he worked at the Italian Institute of Metrology Research (INRiM). Since February 2023, he has been an Assistant Professor (RTD-A) with the Department of Electronics and Telecommunications (DET), Politecnico di Torino. His research interests include optical communication systems, digital signal processing for optical transceivers, and performance monitoring of high-speed optical networks.



Akanksha Bhutani (Senior Member, IEEE) earned her M.Sc. and Ph.D. degrees in Electrical Engineering and Information Technology from the Karlsruhe Institute of Technology (KIT), Germany, in 2012 and 2019, respectively. In January 2026, she joined Infineon Technologies Austria AG as a Senior Staff EDA Engineer for Simulation Methodology in the R&D department, where she is currently working on simulation methodologies for quantum computing systems and artificial intelligence and machine learning-based approaches for electromagnetic simulations. From 2012 to 2025, she worked as a Research Associate at the Institute of Radio Frequency Engineering and Electronics (IHE), KIT, and from 2021 to 2025, she served as Research Group Leader of the Antennas and Packaging Group at IHE, KIT. During this period, her work focused on millimeter-wave and sub-THz antennas and packaging solutions for next-generation radar and wireless communication systems. She has received several awards for her scientific contributions, including the Carl Freudenberg Prize (2019), the Südwestmetall Advancement Award for Young Researchers (2020), the IEEE Microwave Magazine Best Paper Award (awarded in 2019), the European Microwave Week (EuMW) Best Paper Awards in 2019 (first author) and 2022 (second author), and the International IHP "Wolfgang Mehr" Fellowship Award from the Leibniz Institute for Innovative Microelectronics (IHP) in 2023. In 2023, she served as Operations Officer for the European Microwave Week (EuMW) 2023, held in Berlin. She has authored and co-authored more than 35 articles in peer-reviewed scientific journals and over 55 papers in peer-reviewed conference proceedings.



Anna-Chiara Hilkert received the B.Sc. and M.Sc. degrees in Biomedical Engineering from the University of Applied Sciences Mannheim in 2023 and 2025, respectively. In 2025, she joined the Institute of Radio Frequency Engineering and Electronics (IHE) at the Karlsruhe Institute of Technology (KIT) as a Research Assistant. Her research focuses on antenna design, multi-chip interconnects, and packaging technologies for optical and terahertz-frequency signals in next-generation wireless communication systems.



Md Salek Mahmud received the B.Sc. degree in Electrical Engineering from the Islamic University of Technology, Dhaka, Bangladesh, in 2012, the M.Sc. degree in Optics and Photonics from the Karlsruhe Institute of Technology (KIT), Karlsruhe, Germany, in 2017, and the Ph.D. degree in Electrical Engineering from KIT in 2025. He is currently continuing his work as a Postdoctoral Research Associate at KIT. His research interests include optical communication systems, hybrid optical-electronic systems and real-time digital signal processing.



Filipp Gostner received his Bachelor's degree in Physics from the Karlsruhe Institute of Technology (KIT) in 2024 and is currently pursuing a Master's degree in Physics at KIT, specializing in solid-state physics and optics. His research interests include digital signal processing for high-speed optical and wireless communication systems, with a focus on real-time FPGA-based signal processing for coherent optical and sub-THz communication links.

This work is licensed under a Creative Commons Attribution 4.0 License. For more information, see https://creativecommons.org/licenses/by/4.0/

This article has been accepted for publication in IEEE Transactions on Terahertz Science and Technology. This is the author's version which has not been fully edited and content may change prior to final publication. Citation information: DOI 10.1109/TTHZ.2026.3749414



Axel Tessmann received the Dipl.-Ing. degree in electrical engineering from the University of Karlsruhe, Germany, in 1997 and the Ph.D. degree in electrical engineering from the University of Karlsruhe, Germany, in 2006. In 1997, he joined the Microelectronics Department, Fraunhofer Institute for Applied Solid State Physics (IAF), Freiburg, Germany, where he is involved in the development of monolithically integrated circuits and subsystems for high-resolution imaging systems and high data rate wireless communication links. His main research areas are the design and packaging of millimeter-wave and submillimeter wave ICs as well as circuit simulation and linear and nonlinear device modeling. He is currently Group Manager of the millimeter wave packaging and subsystem group at the Fraunhofer IAF.



Sandrine Wagner received a B.Sc. in Electronics and Informatics from the University of Mulhouse, France in 1989. She joined Micronas GmbH in Freiburg, Germany in 1989 where she was responsible for layout and physical verification of large scale integrated semi-conductor devices. In 2010 she joined the Fraunhofer Institute for Applied Solid State Physics (IAF), Freiburg, Germany. Her main interest is the measurement of high frequency nonlinear circuits.



Lisa Nolte was born in Karlsruhe, Germany, in 1994. She completed her vocational training as an industrial mechanic at the Karlsruhe Institute of Technology (KIT) from 2014 to 2017. In 2019, she joined the Institute of Photonic and Quantum Electronics (IPQ) at KIT as a technical staff member, where she is responsible for optical and electronic packaging.



Haizheng Li received the B.Eng. degree in Automation from the Beijing Institute of Technology, Beijing, China, in 2017, and the M.Sc. degree in Electrical Engineering and Information Technology (ETIT) from the Karlsruhe Institute of Technology (KIT), Karlsruhe, Germany, in 2021. He is currently pursuing the Ph.D. degree with the Communications Engineering Laboratory, Karlsruhe Institute of Technology. His research interests include spatially coupled low-density parity-check (SC-LDPC) codes, and channel coding for optical communication.



Christian Koos received the Ph.D. (Dr.-Ing.) degree in electrical engineering from the University of Karlsruhe, Karlsruhe, Germany, in 2007. He is currently a full Professor with the Karlsruhe Institute of Technology, Karlsruhe, Germany, where he is heading the Institute of Photonics and Quantum Electronics. He has co-founded several start-up companies, such as Vanguard Photonics GmbH, Vanguard Automation GmbH, SilOriX GmbH, and DeepLight SA. From 2008 to 2010, he was affiliated with the Corporate Research and Technology Department of Carl Zeiss AG in Oberkochen, Germany, where he led the technology forecast in the area of nanotechnology. He is the author of more than 140 journal papers and more than 30 patent families. His research interests include silicon photonics and hybrid integration concepts along with the associated applications in high-speed communications, optical sensing and metrology, and ultra-fast photonic-electronic signal processing. He was the recipient of several research awards and prestigious grants, such as the ERC Starting Grant in 2011 and ERC Consolidator Grant in 2017.



Thomas Zwick (Fellow, IEEE) received the Dipl.-Ing. (M.S.E.E.) and the Dr.-Ing. (Ph.D.E.E.) degrees from the University Karlsruhe (TH), Germany, in 1994 and 1999, respectively. From 1994 to 2001 he was a research assistant at the Institut für Hochstfrequenztechnik und Elektronik (IHE) at the University Karlsruhe (TH), Germany. In February 2001 he joined IBM as research staff member at the IBM T. J. Watson Research Center, Yorktown Heights, NY, USA. From October 2004 to September 2007, Thomas Zwick was with Siemens AG, Lindau, Germany. During this period he managed the RF development team for automotive radars. In October 2007, he became a full professor at the Karlsruhe Institute of Technology (KIT), Germany. He is the director of the Institut für Hochfrequenztechnik und Elektronik (IHE) at the KIT.



Laurent Schmalen (Fellow, IEEE) received the Dipl.-Ing. degree in electrical engineering and information technology and the Dr.-Ing. degree from RWTH Aachen University, Germany, in 2005 and 2011, respectively. From 2011 to 2019, he was with Alcatel-Lucent Bell Laboratories and Nokia Bell Laboratories. From 2014 to 2019, he was also a Guest Lecturer with the University of Stuttgart, Stuttgart, Germany. Since 2019, he has been a Full Professor with Karlsruhe Institute of Technology, where he co-heads the Communications Engineering Laboratory. His research interests include channel coding, modulation formats, and optical communications. He was a recipient and a co-recipient of several awards, including the E-Plus Award for his Ph.D. thesis, the 2013 Best Student Paper Award from the IEEE Signal Processing Systems Workshop, the 2016 and 2018 Journal of Lightwave Technology Best Paper Awards, and a Bell Laboratories President Award. He served as an Associate Editor for IEEE TRANSACTIONS ON COMMUNICATIONS between 2021 and 2026.



Sebastian Randel (Senior Member, IEEE) received the Dr.-Ing. degree for his work on high-speed optical-time-division-multiplexed transmission systems from Technische Universität Berlin, Berlin, Germany, in 2005. He is currently a full Professor with the Karlsruhe Institute of Technology, Karlsruhe, Germany, where he is co-heading the Institute of Photonics and Quantum Electronics. From 2005 to 2010, he was a Research Scientist with Siemens Corporate Technology, Munich, Germany, where he led research and standardization activities in the fields of polymer-optical-fiber communications, visible-light communications, and optical access networks. From 2010 to 2016, he was a Member of Technical Staff with Bell Laboratories, Holmdel, NJ, USA. His current research focuses on high-capacity power-efficient optical and sub-THz communication systems and networks.

This work is licensed under a Creative Commons Attribution 4.0 License. For more information, see https://creativecommons.org/licenses/by/4.0/